PHYSICAL REVIEW D **92,** 116005 (2015)

Double Higgs boson production and decay in Randall-Sundrum model at hadron colliders

Zhang Wen-Juan,[1] Ma Wen-Gan,[1] Zhang Ren-You,[1] Li Xiao-Zhou,[1] Guo Lei,[2] and Chen Chong[1]

[1]*Department of Modern Physics, University of Science and Technology of China, Hefei, Anhui 230026, People's Republic of China*

[2]*Department of Physics, Chongqing University, Chongqing 401331, People's Republic of China*

(Received 4 July 2015; published 11 December 2015)

We investigate the double Higgs production and decay at the 14 TeV LHC and 33 TeV HE-LHC in both the standard model (SM) and Randall-Sundrum (RS) model. In our calculation we consider reasonably only the contribution of the lightest two Kaluza-Klein (KK) gravitons. We present the integrated cross sections and some kinematic distributions in both models. Our results show that the RS effect in the vicinities of $M_{HH} \sim M_1$, M_2 (the masses of the lightest two KK gravitons) or in the central Higgs rapidity region is quite significant, and can be extracted from the heavy SM background by imposing proper kinematic cuts on final particles. We also study the dependence of the cross section on the RS model parameters, the first KK graviton mass M_1, and the effective coupling c_0, and find that the RS effect is reduced obviously with the increment of M_1 or decrement of c_0.

DOI: 10.1103/PhysRevD.92.116005 PACS numbers: 11.10.Kk, 12.38.Bx

I. INTRODUCTION

The huge gauge hierarchy between the Planck scale and electroweak (EW) scale in the standard model (SM) motivates the proposal of new physics beyond the SM. Among amounts of prospective candidates addressing the hierarchy problem, extra dimension models stay distinctive by taking into consideration the gravity effects at TeV scale. There are two distinct mechanisms to eliminate the gauge scale disparity in the higher dimensions scenario, the large extra dimensions (LED) model, also known as the Arkani-Hamed-Dimopoulos-Dvali (ADD) model [1], and the Randall-Sundrum (RS) model [2].

In the scenario of the ADD model, the spacetime is constituted by $D = 4 + n$ dimensions. The graviton can travel in the D-dimensional bulk while the SM particles are constrained to the normal $(3 + 1)$-dimensional brane. The D-dimensional fundamental scale M_D is related to the effective four-dimensional Planck scale $M_{\rm Pl}$ via $M_{\rm Pl}^2 \sim M_D^{n+2} R^n$, where R is the radius of the compactification torus of the extra n dimensions. If R is large enough, the fundamental scale can be around the EW scale (i.e., $M_D \sim$ TeV); therefore, the gauge hierarchy problem is solved. However, the ADD model reintroduces a new hierarchy between the compactification scale $R^{-1} \sim$ eV − MeV and the fundamental scale $M_D \sim$ TeV. In the scenario of the RS model, there is only one extra spacial dimension, which is compactified to an orbifold of the size of the order of $M_{\rm Pl}^{-1}$. The spacetime in the RS model is warped and has a metric multiplied by an exponential factor that arises from the background AdS_5 spacetime. The gauge hierarchy problem is solved by the exponential factor and the new hierarchy in the ADD model is also avoided. Moreover, the distinct characteristic of the Kaluza-Klein (KK) graviton spectrum differing from that in the ADD model will lead to rich phenomenology at TeV colliders.

The discovery of a new neutral boson with mass of $M_H \sim 126$ GeV, which has promise to be the SM Higgs boson, has been announced by both the ATLAS and CMS collaborations at the CERN Large Hadron Collider (LHC) [3]. It is of great interest for physicists to probe the newfound particle's properties to verify whether it is the SM Higgs boson or the content of new physics. Moreover, the measurement of couplings of the Higgs boson with other particles as well as itself is desired to understand the mechanism of electroweak symmetry breaking. The double Higgs boson production provides an opportunity to probe the Higgs trilinear self interaction and therefore reconstruct the Higgs potential.

Up to now, the double Higgs boson production at the LHC in the SM including the next-to-leading order (NLO) QCD corrections has been calculated in Ref. [4]. The evaluation for the next-to-next-to-leading order (NNLO) QCD corrections to SM Higgs boson pair production at hadron colliders within the large top-mass approximation can be found in Ref. [5]. The Higgs boson pair production at hadron colliders beyond the SM has also been explored, such as in the SM with four generation quarks [6], littlest Higgs model [7], universal extra dimensions model [8] and supersymmetry as well as the LED model [9,10]. In addition, the Higgs boson pair production via vector boson fusion has been studied up to the QCD NNLO in the SM [11] and type-II two-Higgs-doublet model [12].

In this paper, we study the possible RS effect on double Higgs boson production at hadron colliders. The rest of this paper is organized as follows: In Sec. II we give a brief description of the RS model. The calculation setup of related subprocesses is presented in Sec. III. In Sec. IV we present the numerical results and discussion. Finally, we give a short summary in Sec. V. The relevant Feynman rules are given in the appendix.

II. RELATED THEORY

The spacetime in the RS model is assumed to be a five-dimensional bulk constituted of the $(3+1)$-dimensional Minkowski spacetime and a warped extra dimension that is compactified on an orbifold S_1/Z_2 with compactification radius R_c. At the fixed points $\phi = 0$ and π of the orbifold, two branes with opposite tensions, the ultraviolet (UV) brane (Planck brane) and the infrared (IR) brane (TeV brane), are set, respectively. It is assumed that the graviton propagates in the whole bulk while the SM particles are localized on the IR brane. By solving the corresponding five-dimensional Einstein field equation, we get a non-factorizable metric of the bulk as

$$ds^2 = e^{-2kR_c|\phi|}\eta_{\mu\nu}dx^\mu dx^\nu + {R_c}^2 d\phi^2, \qquad (2.1)$$

where $0 \le |\phi| \le \pi$, $\eta_{\mu\nu}$ represents the ordinary Minkowski metric, and $k \sim \mathcal{O}(M_{\rm Pl})$ is the curvature scale of AdS_5. The hierarchy between the Planck scale and EW scale is therefore generated by the exponential warp factor $e^{-kR_c\pi}$ via the relationship $M_{\rm Pl}e^{-kR_c\pi} \sim \mathcal{O}(\mathrm{TeV})$ requiring not too large R_c. To explore the gravity effects on the TeV brane at $\phi = \pi$, one can expand the graviton field, treated as the fluctuation around the background metric, into the RS KK modes $h_{\mu\nu}^{(n)}$ upon compactification. Then the effective four-dimensional interaction Lagrangian of the RS model is given by [13]

$$\mathcal{L} = -\frac{1}{\overline{M}_{\rm Pl}}T^{\mu\nu}h_{\mu\nu}^{(0)} - \frac{1}{\Lambda_\pi}T^{\mu\nu}\sum_{n=1}^{\infty}h_{\mu\nu}^{(n)}, \qquad (2.2)$$

where $\Lambda_\pi = \overline{M}_{\rm Pl}e^{-kR_c\pi}$, $\overline{M}_{\rm Pl} = M_{\rm Pl}/\sqrt{8\pi}$ is the reduced Planck scale, and $T^{\mu\nu}$ represents the SM energy-momentum tensor. The couplings of the zero mode $(n = 0)$ and massive modes $(n = 1, 2, \ldots)$ to SM particles are proportional to $1/\bar{M}_{\rm Pl}$ and $1/\Lambda_\pi$, respectively. Because of the fact that $\Lambda_\pi/\overline{M}_{\rm Pl} \sim \mathcal{O}(10^{-16})$, the zero mode decouples from the graviton mass spectrum. The mass of the n^{th} RS KK graviton can be written as

$$M_n = x_n k e^{-kR_c\pi} = \frac{x_n}{x_1}M_1, \qquad (2.3)$$

where x_n is the nth root of the Bessel function, e.g., $x_1 \simeq 3.83$, $x_2 \simeq 7.02$, and $x_3 \simeq 10.17$. The mass splitting of the RS KK gravitons is of the TeV order, which implies that the RS KK gravitons can be produced as resonances at multi-TeV colliders.

In this paper we choose the mass of the first KK mode M_1 and the effective coupling constant $c_0 \equiv k/\overline{M}_{\rm Pl}$ as the two independent input parameters of the RS model. The relevant Feynman rules of RS KK graviton couplings to SM particles [14] are presented in the appendix. The effective graviton propagator, defined as a sum over an infinite tower of RS KK gravitons, in the de Donder gauge can be expressed as

$$G_{KK}^{\mu\nu,\alpha\beta} = \frac{1}{2}D(s)\left(\eta^{\mu\alpha}\eta^{\nu\beta} + \eta^{\mu\beta}\eta^{\nu\alpha} - \frac{2}{3}\eta^{\mu\nu}\eta^{\alpha\beta}\right), \qquad (2.4)$$

where

$$D(s) = \sum_{n=1}^{\infty}\frac{i}{s - M_n^2 + iM_n\Gamma_n}, \qquad (2.5)$$

and Γ_n is the total decay width of the nth KK graviton written as [15,16]

$$\Gamma_n = \frac{1}{16\pi}x_n^2 M_n c_0^2 \Delta_n, \qquad (2.6)$$

with

$$\Delta_n = \Delta_n^{\gamma\gamma} + \Delta_n^{gg} + \Delta_n^{WW} + \Delta_n^{ZZ} + \sum_\nu \Delta_n^{\nu\nu} + \sum_l \Delta_n^{ll} + \sum_q \Delta_n^{qq} + \Delta_n^{HH}. \qquad (2.7)$$

Δ_n^{yy} is the coefficient for the decay $G_{KK}^{(n)} \to yy$, and y is the SM particle involved. The explicit expressions for $\Delta_n^{yy}(y = \gamma, g, W, Z, \nu, l, q, H)$ are given in Refs. [15,17].

III. CALCULATION SETUP

In our calculation we set the quark masses of the first two generations to zero, i.e., $m_u = m_c = m_d = m_s = 0$, and consequently only consider top- and bottom-quark Yukawa couplings with a Higgs boson. We use the dimensional regularization scheme in $D = 4 - 2\epsilon$ dimensions to isolate UV and IR singularities and adopt the five-flavor scheme in the convolution with parton distribution functions (PDFs).

A. Double Higgs boson production in the SM

Because of the masslessness of the first two generations of quarks, the dominant contribution to the Higgs boson pair production at a high energy hadron collider in the SM is from the gg fusion and $b\bar{b}$ annihilation partonic processes. Although the lowest order amplitude squared for $gg \to HH$ is of the $\mathcal{O}(\alpha_{ew}^2\alpha_s^2)$, which is 2 orders of magnitude in α_s higher than that for $b\bar{b} \to HH$, the gg fusion subprocess can be dominant channel at TeV-scale hadron colliders due to the high gluon luminosity. In this paper we consider the $gg \to HH$ and $b\bar{b} \to HH$ partonic processes only at the lowest order for the hadronic production of the Higgs boson pair in the SM.

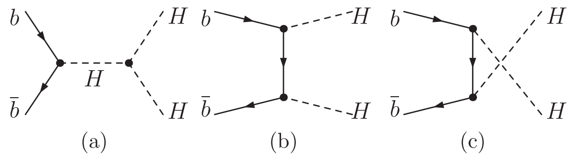

FIG. 1. The tree-level Feynman diagrams for the $b\bar{b} \to HH$ partonic process in the SM.

1. Bottom-antibottom annihilation

The leading order (LO) contribution from the $b\bar{b} \to HH$ channel at a high energy hadron collider in the SM is much less than from the $gg \to HH$ channel, e.g., the LO contributions from $b\bar{b} \to HH$ to the total cross section at the 14 TeV LHC and 33 TeV HE-LHC are less than 0.185% and 0.163%, respectively. Therefore, it is reasonable to include only the lowest order contribution for the $b\bar{b} \to HH$ channel in the SM calculation. The tree-level Feynman diagrams for the $b\bar{b} \to HH$ partonic process in the SM are shown in Fig. 1. The cross section for $b\bar{b} \to HH$ is expressed as

$$\hat{\sigma}^{b\bar{b}}_{\rm SM}(\hat{s}) = \frac{1}{2}\frac{1}{4}\frac{1}{9}\frac{(2\pi)^4}{4|\vec{p}|\sqrt{\hat{s}}}\int \sum_{\rm spin}\sum_{\rm color}|\mathcal{M}^{0,b\bar{b}}_{\rm SM}|^2 d\Omega_2, \qquad (3.1)$$

where $\vec{p}$ is the three-momentum of one of the incoming partons in the center-of-mass system, $\mathcal{M}^{0,b\bar{b}}_{\rm SM}$ is the Feynman amplitude for the tee-level diagrams in Fig. 1, and $d\Omega_2$ is the two-body phase space element. The first factor $\frac{1}{2}$ is due to the two identical Higgs bosons of final state, and the following two factors $\frac{1}{4}$ and $\frac{1}{9}$ are from the averaging of spins and colors of initial state.

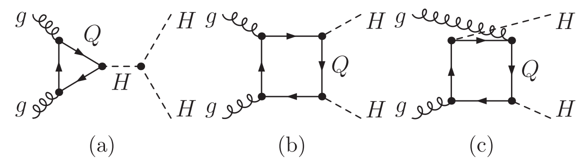

FIG. 2. The lowest-level Feynman diagrams for the $gg \to HH$ partonic process in the SM, where Q represents massive quarks t and b. (The diagrams with the exchange of initial and/or final identical particles are not shown.)

2. Gluon-gluon fusion

In Fig. 2 we demonstrate some representative Feynman diagrams at the lowest order for the $gg \to HH$ partonic process in the SM. They are all one-loop graphs and the full one-loop amplitude for this partonic process, $\mathcal{M}^{1,gg}_{\rm SM}$, is UV and IR safe. The cross section for $gg \to HH$ at the lowest order, $\hat{\sigma}^{gg}_{\rm SM}$, can be expressed as

$$\hat{\sigma}^{gg}_{\rm SM}(\hat{s}) = \frac{1}{2}\frac{1}{4}\frac{1}{64}\frac{(2\pi)^4}{4|\vec{p}|\sqrt{\hat{s}}}\int \sum_{\rm spin}\sum_{\rm color}|\mathcal{M}^{1,gg}_{\rm SM}|^2 d\Omega_2. \qquad (3.2)$$

3. Integrated cross section

We denote $\sigma^{b\bar{b}}_{\rm SM}$ and $\sigma^{gg}_{\rm SM}$ as the integrated cross sections for $pp \to b\bar{b} \to HH + X$ and $pp \to gg \to HH + X$ in the SM, respectively. The two integrated cross sections can be obtained by convoluting the parton-level cross sections, $\hat{\sigma}^{b\bar{b}}_{\rm SM}$ and $\hat{\sigma}^{gg}_{\rm SM}$, with the corresponding PDFs,

$$\begin{aligned}\sigma^{b\bar{b}}_{\rm SM} &= \int_0^1 dx_1 \int_0^1 dx_2 [G_{b/P_1}(x_1,\mu_f)G_{\bar{b}/P_2}(x_2,\mu_f) + (1 \leftrightarrow 2)]\hat{\sigma}^{b\bar{b}}_{\rm SM}(\hat{s} = x_1x_2s),\\ \sigma^{gg}_{\rm SM} &= \frac{1}{2}\int_0^1 dx_1 \int_0^1 dx_2 [G_{g/P_1}(x_1,\mu_f)G_{g/P_2}(x_2,\mu_f) + (1 \leftrightarrow 2)]\hat{\sigma}^{gg}_{\rm SM}(\hat{s} = x_1x_2s),\end{aligned} \qquad (3.3)$$

where $G_{b,\bar{b},g/P}$ are the PDFs of bottom, antibottom and gluon in proton, $x_i (i = 1, 2)$ is the momentum fraction of a parton in proton P_i, and μ_f is the factorization scale. Then the integrated cross section for the parent process $pp \to HH + X$ in the SM is obtained as

$$\sigma_{\rm SM} = \sigma^{gg}_{\rm SM} + \sigma^{b\bar{b}}_{\rm SM}. \qquad (3.4)$$

B. Double Higgs boson production in the RS model

In the framework of the RS model, the Higgs boson pair can be produced via virtual KK graviton exchange, i.e.,

$$pp \to gg/q\bar{q} \to G_{KK} \to HH + X, \qquad (q = u, d, c, s, b), \qquad (3.5)$$

in addition to the production mechanism in the SM mentioned in Sec. III A.

1. Tree-level contribution

In the SM, only the $b\bar{b}$ annihilation can give a tree-level contribution to the Higgs pair production at a hadron collider. However, in the RS model both the gg fusion and all the $q\bar{q}(q = u, d, c, s, b)$ annihilations can contribute at tree level to the Higgs pair production via KK graviton mediation, since the graviton field can couple with SM

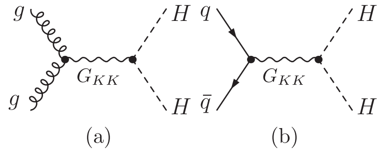

FIG. 3. The tree-level Feynman diagrams for $gg/q\bar{q} \to G_{KK} \to HH$, where $q = u, d, c, s, b$, and G_{KK} represents the KK graviton.

particles. The tree-level Feynman diagrams for $gg/q\bar{q} \to G_{KK} \to HH(q = u, d, c, s, b)$ are presented in Fig. 3. The Feynman amplitudes for Figs. 3(a)–3(b) are denoted as $\mathcal{M}^{0,gg}_{KK}$ and $\mathcal{M}^{0,q\bar{q}}_{KK}$, respectively. Therefore, the tree-level amplitudes for the gg fusion and $q\bar{q}$ annihilation subprocesses in the RS model are

$$\begin{aligned} \mathcal{M}^{0,gg}_{\rm RS} &= \mathcal{M}^{0,gg}_{KK} \quad (gg\,\text{fusion}), \\ \mathcal{M}^{0,q\bar{q}}_{\rm RS} &= \mathcal{M}^{0,q\bar{q}}_{KK} \quad (q\bar{q}\,\text{annihilation}, q = u, d, c, s), \\ \mathcal{M}^{0,b\bar{b}}_{\rm RS} &= \mathcal{M}^{0,b\bar{b}}_{\rm SM} + \mathcal{M}^{0,b\bar{b}}_{KK} \quad (b\bar{b}\,\text{annihilation}). \end{aligned} \tag{3.6}$$

We denote the tree-level cross sections for $gg \to HH$ and $q\bar{q} \to HH$ in the RS model as $\hat{\sigma}^{0,gg}_{\rm RS}$ and $\hat{\sigma}^{0,q\bar{q}}_{\rm RS}$, respectively.

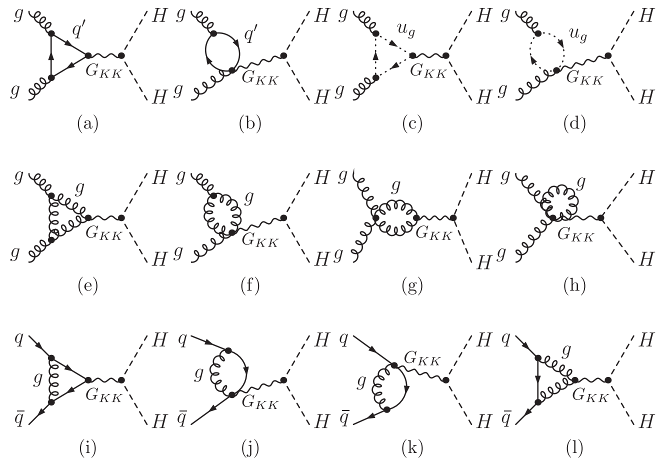

FIG. 4. The QCD one-loop Feynman diagrams for $gg/q\bar{q} \to G_{KK} \to HH(q = u, d, c, s)$, where u_g is the ghost for gluon, G_{KK} represents the KK graviton, and q' in fermion loops runs over u, d, c, s, t, b. (The diagrams with the exchange of the initial two gluons are not shown.)

Since the loop contribution from the SM-like diagrams (shown in Fig. 2) for the gg fusion subprocess is rather large, we include $\hat{\sigma}^{gg}_{\rm SM}$ in the lowest order integrated cross section for the parent process $pp \to HH + X$ and therefore obtain

$$\begin{aligned} \sigma^0_{\rm RS} &= [\sigma^{gg}_{\rm SM} + \sigma^{0,gg}_{\rm RS}] + \sum_{q=u,d}^{c,s,b} \sigma^{0,q\bar{q}}_{\rm RS} \\ &= \frac{1}{2}\int_0^1 dx_1 \int_0^1 dx_2 [G_{g/P_1}(x_1,\mu_f) G_{g/P_2}(x_2,\mu_f) + (1 \leftrightarrow 2)][\hat{\sigma}^{gg}_{\rm SM}(\hat{s} = x_1 x_2 s) + \hat{\sigma}^{0,gg}_{\rm RS}(\hat{s} = x_1 x_2 s)] \\ &\quad + \sum_{q=u,d}^{c,s,b} \int_0^1 dx_1 \int_0^1 dx_2 [G_{q/P_1}(x_1,\mu_f) G_{\bar{q}/P_2}(x_2,\mu_f) + (1 \leftrightarrow 2)]\hat{\sigma}^{0,q\bar{q}}_{\rm RS}(\hat{s} = x_1 x_2 s). \end{aligned} \tag{3.7}$$

2. NLO QCD corrections

Because of the smallness of bottom-quark density in the proton compared with the gluon and light quarks, the LO cross sections contributed by the $b\bar{b} \to HH$ subprocess at the LHC and HE-LHC in the RS model are less than 0.181% and 0.153%, respectively. Therefore, we include only the LO contribution in the calculation of the $b\bar{b} \to HH$ subprocess in the RS model. Some representative QCD one-loop diagrams for $gg/q\bar{q} \to HH(q = u, d, c, s)$ involving KK graviton exchange are shown in Fig. 4. The full one-loop amplitudes for the $gg \to HH$ and $q\bar{q} \to HH(q = u, d, c, s)$ partonic processes in the RS model can be written as

$$\begin{aligned} \mathcal{M}^{1,gg}_{\rm RS} &= \mathcal{M}^{1,gg}_{\rm SM} + \mathcal{M}^{1,gg}_{KK} \quad (gg\,\text{fusion}), \\ \mathcal{M}^{1,q\bar{q}}_{\rm RS} &= \mathcal{M}^{1,q\bar{q}}_{KK} \quad (q\bar{q}\,\text{annihilation}, q = u, d, c, s), \end{aligned} \tag{3.8}$$

where $\mathcal{M}^{1,gg}_{KK}$ and $\mathcal{M}^{1,q\bar{q}}_{KK}$ are the one-loop amplitudes for $gg \to G_{KK} \to HH$ and $q\bar{q} \to G_{KK} \to HH$, respectively. In order to deal with the UV divergences, we introduce the quark and gluon wave-function renormalization constants as follows:

$$q^{(\rm bare)}_{L,R} = \left(1 + \frac{1}{2}\delta Z^q_{L,R}\right) q_{L,R}, \qquad G^{a(\rm bare)}_\mu = \left(1 + \frac{1}{2}\delta Z^G\right) G^a_\mu. \tag{3.9}$$

By adopting the on-shell renormalization scheme, these renormalization constants are fixed as

$$\delta Z^q_{L,R} = -\frac{\alpha_s(\mu_r)}{4\pi} C_F(\Delta_{\rm UV} - \Delta_{\rm IR}), \qquad (q = u, d, c, s),$$
$$\delta Z^G = -\frac{\alpha_s(\mu_r)}{4\pi}\left[\left(\frac{4}{3}n_f^{\rm UV} T_F - \frac{5}{3}C_A\right)\Delta_{\rm UV} - \left(\frac{4}{3}n_f^{\rm IR} T_F - \frac{5}{3}C_A\right)\Delta_{\rm IR}\right] - \frac{\alpha_s(\mu_r)}{6\pi}\left[\ln\frac{\mu_r^2}{m_t^2} + \ln\frac{\mu_r^2}{m_b^2}\right], \tag{3.10}$$

where $C_F = \frac{4}{3}$, $C_A = 3$, $T_F = \frac{1}{2}$, μ_r is the renormalization scale, $\Delta_{\rm UV,IR} = \frac{1}{\epsilon_{\rm UV,IR}} - \gamma_E + \ln 4\pi$ are UV and IR regulators, $n_f^{\rm UV} = 6$ corresponds to the six flavors of quarks, and $n_f^{\rm IR} = 4$ is the number of massless quarks. After performing the renormalization procedure the UV singularities are removed, and therefore the NLO QCD virtual corrections to the $gg \to HH$ and $q\bar{q} \to HH(q = u, d, c, s)$ partonic processes in the RS model, $\hat{\sigma}^{gg,V}_{\rm RS}$ and $\hat{\sigma}^{q\bar{q},V}_{\rm RS}(q = u, d, c, s)$, are UV finite.

The renormalized virtual corrections are UV finite, but still contain soft (S) and collinear (C) IR singularities, which can be canceled by adding the contributions of the related real emission processes and PDF counterterms. The real gluon emission partonic processes, $gg/q\bar{q} \to HHg(q = u, d, c, s)$, have both soft and collinear IR singularities that can be separated by applying the two cutoff phase space slicing (TCPSS) method [18]. Two cutoffs δ_s and δ_c are introduced in the TCPSS method to divide the phase space into S, hard collinear (HC) and hard noncollinear ($\overline{HC}$) regions. Then the cross sections for the real gluon emission partonic processes can be expressed as

$$\hat{\sigma}^{ab,R}_{\rm RS} = \hat{\sigma}^{ab,S}_{\rm RS} + \hat{\sigma}^{ab,HC}_{\rm RS} + \hat{\sigma}^{ab,\overline{HC}}_{\rm RS}, \tag{3.11}$$

where $ab = gg, q\bar{q}$ correspond to the gg fusion and $q\bar{q}$ annihilation, respectively. The hard noncollinear cross section $\hat{\sigma}^{ab,\overline{HC}}_{\rm RS}$ is IR finite, and the soft IR singularity in $\hat{\sigma}^{ab,S}_{\rm RS}$ can be canceled exactly by that in the virtual correction $\hat{\sigma}^{ab,V}_{\rm RS}$ as demonstrated by the Kinoshita-Lee-Nauenberg theorem [19]. The collinear IR singularity in $\hat{\sigma}^{ab,HC}_{\rm RS}$ is partially canceled by that in the virtual correction $\hat{\sigma}^{ab,V}_{\rm RS}$, and the remaining collinear divergence can be absorbed by the corresponding PDF counterterms. Then the full NLO QCD corrections to the $gg \to HH$ and $q\bar{q} \to HH(q = u, d, c, s)$ partonic processes in the RS model are obtained as

$$\Delta\hat{\sigma}^{ab}_{\rm RS} = \hat{\sigma}^{ab,V}_{\rm RS} + \hat{\sigma}^{ab,R}_{\rm RS} + \hat{\sigma}^{ab,{\rm PDF}}_{\rm RS}, \qquad (ab = gg, q\bar{q}), \tag{3.12}$$

where $q = u, d, c, s$ and the superscripts V, R, PDF represent the virtual, real, and PDF counterterm contributions, respectively.

The real light-quark emission partonic processes, $gq \to HHq$ and $g\bar{q} \to HH\bar{q}(q = u, d, c, s)$, contain only collinear IR singularities. We separate the phase space into C and noncollinear regions by using the cutoff δ_c. The collinear IR singularities in the real light-quark emissions are also canceled by the PDF counterterms. Then we obtain the corrections from the real light-quark emissions and corresponding PDF counterterms as[1]

$$\Delta\hat{\sigma}^{gq}_{\rm RS} = \hat{\sigma}^{gq,R}_{\rm RS} + \hat{\sigma}^{gq,{\rm PDF}}_{\rm RS},$$
$$\Delta\hat{\sigma}^{g\bar{q}}_{\rm RS} = \hat{\sigma}^{g\bar{q},R}_{\rm RS} + \hat{\sigma}^{g\bar{q},{\rm PDF}}_{\rm RS}, \qquad (q = u, d, c, s). \tag{3.13}$$

The PDF counterterm contributions in Eqs. (3.12)–(3.13) can be expressed as

$$\hat{\sigma}^{gg,{\rm PDF}}_{\rm RS} = 2P_{gg} \otimes \hat{\sigma}^{0,gg}_{\rm RS}, \qquad \hat{\sigma}^{q\bar{q},{\rm PDF}}_{\rm RS} = 2P_{qq} \otimes \hat{\sigma}^{0,q\bar{q}}_{\rm RS},$$
$$\hat{\sigma}^{gq,{\rm PDF}}_{\rm RS} = \hat{\sigma}^{g\bar{q},{\rm PDF}}_{\rm RS} = P_{gq} \otimes \hat{\sigma}^{0,gg}_{\rm RS} + P_{qg} \otimes \hat{\sigma}^{0,q\bar{q}}_{\rm RS}. \tag{3.14}$$

P_{gg}, P_{qq}, P_{gq}, and P_{qg} are the QCD splitting functions [18],

$$P_{gg}(z) = 6\left[\frac{z}{1-z} + \frac{1-z}{z} + z(1-z)\right],$$
$$P_{qq}(z) = C_F\frac{1+z^2}{1-z},$$
$$P_{gq}(z) = C_F\frac{1+(1-z)^2}{z},$$
$$P_{qg}(z) = T_F[z^2 + (1-z)^2], \tag{3.15}$$

and the "⊗-convolution" is defined as

$$[P \otimes \hat{\sigma}](\hat{s}) = \frac{1}{\epsilon}\left[\frac{\alpha_s}{2\pi}\frac{\Gamma(1-\epsilon)}{\Gamma(1-2\epsilon)}\left(\frac{4\pi\mu_r^2}{\mu_f^2}\right)^{\epsilon}\right]\int_0^1 dz P(z)\hat{\sigma}(z\hat{s}). \tag{3.16}$$

[1]Because of the charge parity conservation, the real emission correction and corresponding PDF counterterm contribution for $gq \to HHq$ are the same as for $g\bar{q} \to HH\bar{q}$, respectively, i.e., $\hat{\sigma}^{gq,R}_{\rm RS} = \hat{\sigma}^{g\bar{q},R}_{\rm RS}$ and $\hat{\sigma}^{gq,{\rm PDF}}_{\rm RS} = \hat{\sigma}^{g\bar{q},{\rm PDF}}_{\rm RS}$.

3. Integrated cross section

Because of the high gluon luminosity and low bottom-quark density in the proton at the LHC and HE-LHC, we include the $\mathcal{O}(\alpha_{ew}^2\alpha_s^2)$ SM-like contribution [see Eq. (3.2)] to the gg fusion and only consider the tree-level contribution to the $b\bar{b}$ annihilation. Then the integrated cross section for the double Higgs boson production at a pp collider in the RS model can be written as

$$\sigma_{\rm RS} = \sigma_{\rm RS}^0 + \Delta\sigma_{\rm RS}, \tag{3.17}$$

where $\Delta\sigma_{\rm RS}$ is the full NLO QCD correction to the $pp \to HH + X$ process obtained by convoluting the parton-level corrections, $\Delta\hat{\sigma}_{\rm RS}^{gg}$, $\Delta\hat{\sigma}_{\rm RS}^{q\bar{q}}$, $\Delta\hat{\sigma}_{\rm RS}^{gq}$, and $\Delta\hat{\sigma}_{\rm RS}^{g\bar{q}}$, with the corresponding PDFs,

$$\begin{aligned}\Delta\sigma_{\rm RS} = &\sum_{ab\in\mathcal{S}}\frac{1}{1+\delta_{ab}}\int_0^1 dx_1 \\ &\times\int_0^1 dx_2[G_{a/P_1}(x_1,\mu_f)G_{b/P_2}(x_2,\mu_f) \\ &+(1\leftrightarrow 2)]\Delta\hat{\sigma}_{\rm RS}^{ab}(\hat{s}=x_1x_2s), \\ \mathcal{S} = &\{gg, q\bar{q}, gq, g\bar{q}|(q=u,d,c,s)\}.\end{aligned} \tag{3.18}$$

IV. NUMERICAL RESULTS AND DISCUSSION

A. Input parameters

The SM input parameters used in our calculation are taken as [20,21]

$$\begin{aligned}&\alpha_{ew}(0) = 1/137.035999074, \qquad m_t = 173.21\ \text{GeV}, \\ &m_b = 4.75\ \text{GeV}, \\ &M_W = 80.385\ \text{GeV}, \qquad M_Z = 91.1876\ \text{GeV}, \\ &M_H = 126\ \text{GeV}.\end{aligned} \tag{4.1}$$

We checked numerically the independence of the integrated cross section on the two cutoffs δ_s and δ_c, and take $\delta_s = 10^{-4}$ and $\delta_c = \delta_s/50$ in further numerical calculation. We adopt the MSTW2008nlo PDF set [22] with $n_f = 5$ and $\alpha_s(M_Z) = 0.12018$, and set the factorization and renormalization scales being equal for simplicity, i.e., $\mu_f = \mu_r = \mu$. To estimate the theoretical uncertainty from the factorization/renormalization scale, we investigate the scale dependence of the integrated cross sections in both the SM and RS model. In this paper, we take $\mu_0 = M_H$ and $\mu_1 = M_{HH}$ (Higgs pair invariant mass) as two typical central scales.

The theoretical constraint on the effective coupling c_0 in the RS model is $c_0 \in [0.01, 0.1]$ [13]. Up to now, no signature of the RS model has been observed and all the experimental data are in good agreement with the SM predictions, which gives more stringent constraints on the RS model parameters. Recently a lower bound on the first KK graviton mass was given by the ATLAS collaboration at 95% confidence level as $M_1 > 1.23$ and 2.68 TeV for $c_0 = 0.01$ and 0.1, respectively [23]. In the following numerical calculation we take $M_1 = 2.75$ TeV and $c_0 = 0.1$ as the RS model input parameters. Then we obtain the mass of the second KK graviton as $M_2 = 5.04$ TeV from Eq. (2.3).

The effective graviton propagator is a sum over the infinite tower of KK gravitons. Since the KK graviton mass is proportional to the root of the Bessel function, which increases notably, we may apply a cut on the number of active KK gravitons instead of taking the infinite tower of KK gravitons into consideration. We calculate the cross section $\sigma_{\rm RS}^0$ for the Higgs pair production at the 14 TeV LHC and 33 TeV HE-LHC with different numbers of active KK gravitons, and find that the contribution of the nth ($n > 2$) KK gravitons is less than 0.5% and can be neglected. Therefore, in the following calculation we consider only the dominant contribution of the first two KK gravitons.

B. Integrated cross section

In Table I we list the integrated cross sections for $pp \to HH + X$ in the SM and RS model, $\sigma_{\rm SM}$ and $\sigma_{\rm RS}$, at the 14 TeV LHC and 33 TeV HE-LHC. In order to describe the RS effect quantitatively, we define the relative RS effect as $\delta = (\sigma_{\rm RS} - \sigma_{\rm SM})/\sigma_{\rm SM}$. From the table we can see that the relative RS effect is about 3.15% at the 14 TeV LHC, and can reach 14.75% at the 33 TeV HE-LHC, which could be detectable in experiment.

The RS effect is mainly contributed by the KK graviton resonance production when partonic colliding energy is greater than KK graviton mass. In order to enhance the RS effect we apply a lower cut on the invariant mass of the final Higgs boson pair as shown in Table II. In this table we provide the integrated cross sections for $pp \to HH + X$ in both the SM and RS model and the corresponding relative RS effects with the constraint of $M_{HH} > M_{HH}^{\rm cut}$ at the 14 TeV LHC and 33 TeV HE-LHC. We can see clearly that both $\sigma_{\rm SM}$ and $\sigma_{\rm RS}$ decrease, but the relative RS effect increases, with the increment of the Higgs pair invariant mass cut $M_{HH}^{\rm cut}$. For example, the relative RS effects are 3.21% and 14.92% at the 14 TeV LHC and 33 TeV HE-LHC with the constraint of $M_{HH} > 300$ GeV, and

TABLE I. The integrated cross sections for $pp \to HH + X$ in the SM and RS model ($\sigma_{\rm SM}$ and $\sigma_{\rm RS}$) and the corresponding relative RS effects at the 14 TeV LHC and 33 TeV HE-LHC with $\mu = \mu_1$.

$\sqrt{S}$ (TeV)	$\sigma_{\rm SM}(fb)$	$\sigma_{\rm RS}(fb)$	$\delta(\%)$
14	14.8703(9)	15.339(1)	3.15
33	91.509(7)	105.01(1)	14.75

TABLE II. The integrated cross sections ($\sigma_{\rm SM}$, $\sigma^0_{\rm RS}$ and $\sigma_{\rm RS}$) and corresponding relative RS effects for the $pp \to HH + X$ process at the 14 TeV LHC and 33 TeV HE-LHC with $\mu = \mu_1$ for some typical values of $M^{\rm cut}_{HH}$.

$\sqrt{S} = 14$ TeV				
$M^{\rm cut}_{HH}$ (GeV)	$\sigma_{\rm SM}$ (fb)	$\sigma^0_{\rm RS}$ (fb)	$\sigma_{\rm RS}$ (fb)	$\delta(\%)$
300	14.619	14.960	15.088	3.21
400	10.127	10.468	10.595	4.62
500	4.571	4.912	5.038	10.22
600	2.014	2.355	2.479	23.09
700	0.938	1.279	1.403	49.6
800	0.467	0.808	0.931	99.4
900	0.247	0.588	0.711	188
1000	**0.138**	**0.478**	**0.601**	**336**
$\sqrt{S} = 33$ TeV				
$M^{\rm cut}_{HH}$ (GeV)	$\sigma_{\rm SM}$ (fb)	$\sigma^0_{\rm RS}$ (fb)	$\sigma_{\rm RS}$ (fb)	$\delta(\%)$
300	90.30	100.57	103.77	14.92
400	66.24	76.51	79.71	20.33
500	33.35	43.61	46.81	40.36
600	16.44	26.70	29.89	81.81
700	8.54	18.81	21.99	157
800	4.72	14.99	18.17	285
900	2.77	13.03	16.21	485
1000	**1.70**	**11.97**	**15.15**	**791**

increase to 336% and 791%, respectively, after applying the cut of $M_{HH} > 1000$ GeV.

In Table II we list both $\sigma^0_{\rm RS}$ and $\sigma_{\rm RS}$ in the RS model to demonstrate the effect of the NLO QCD correction. We see that the NLO QCD correction always enhances the LO cross section in the RS model; therefore, neglecting the NLO QCD correction would lead to an underestimation of the RS effect. With the increment of $M^{\rm cut}_{HH}$, the NLO QCD correction in the RS model becomes more and more significant, and the production rates for $pp \to HH + X$ in the SM and RS model go down quickly while the relative RS effect increases rapidly. We can read out from the table that the NLO QCD corrected cross section and the relative RS effect are 0.601 fb, 336% at the 14 TeV LHC, and 15.15 fb, 791% at the 33 TeV HE-LHC, respectively, with the constraint of $M_{HH} > 1000$ GeV. In the following calculation we fix the lower cut on the Higgs pair invariant mass as $M^{\rm cut}_{HH} = 1000$ GeV.

In the SM the dominant channel for Higgs pair production at hadron colliders is gluon-gluon fusion via the virtual top quark. This production channel begins at one-loop level; however, the higher order QCD corrections to this process are quite significant. The NLO and NNLO QCD corrections to the SM Higgs pair production at hadron colliders within the large top-mass approximation are already available in Ref. [5]. By using Eqs. (19)–(20) in Ref. [5], we obtain that the NLO and NNLO QCD K-factors for $pp \to gg \to HH + X$ in the SM at the 14 TeV LHC (33 TeV HE-LHC) are 1.873 (1.697) and 2.272 (2.029), respectively. It shows that the NLO and NNLO QCD corrections enhance the LO cross section for the gluon-gluon fusion Higgs pair production channel in the SM significantly. When we take into account these higher order QCD corrections, the relative RS effect will be suppressed by the corresponding QCD K-factor approximately. For example, the relative RS effects at the 14 TeV LHC and 33 TeV HE-LHC for $M^{\rm cut}_{HH} = 1000$ GeV are reduced to about 179% and 466%, respectively, if the NLO QCD corrections to $pp \to gg \to HH + X$ in the SM are taken into consideration.

Table III shows the dependence of the integrated cross section on the factorization/ renormalization scale. We list the integrated cross sections for $pp \to HH + X$ in both the SM and RS model ($\sigma_{\rm SM}$, $\sigma^0_{\rm RS}$, and $\sigma_{\rm RS}$) at the 14 TeV LHC and 33 TeV HE-LHC with $\mu = \mu_0/2$, μ_0, $2\mu_0$, $\mu_1/2$, μ_1, and $2\mu_1$, separately. To estimate the theoretical uncertainty from the factorization/renormalization scale, we define the relative scale uncertainty as $\eta = \frac{\sigma(\mu=\mu_0/2)-\sigma(\mu=2\mu_0)}{\sigma(\mu=\mu_0)}$. Then we obtain $\eta = 72\%$ and 55% in the SM and $\eta = 15\%$ and 11% in the RS model at the 14 TeV LHC and 33 TeV HE-LHC,

TABLE III. The integrated cross sections for the $pp \to HH + X$ process in the SM and RS model at the 14 TeV LHC and 33 TeV HE-LHC for some typical values of the factorization/renormalization scale.

$\sqrt{S} = 14$ TeV						
μ	$\mu_0/2$	μ_0	$2\mu_0$	$\mu_1/2$	μ_1	$2\mu_1$
$\sigma_{\rm SM}$ (fb)	0.52970(9)	0.36887(7)	0.26494(4)	0.18143(3)	0.13764(3)	0.10639(2)
$\sigma^0_{\rm RS}$ (fb)	1.41120(9)	1.07971(7)	0.85104(5)	0.54349(4)	0.47839(3)	0.40561(3)
$\sigma_{\rm RS}$ (fb)	0.9125(8)	0.8554(6)	0.7854(4)	0.6722(4)	0.6014(3)	0.5416(3)
$\sqrt{S} = 33$ TeV						
μ	$\mu_0/2$	μ_0	$2\mu_0$	$\mu_1/2$	μ_1	$2\mu_1$
$\sigma_{\rm SM}$ (fb)	4.9700(8)	3.7642(7)	2.9063(5)	2.1213(4)	1.7011(3)	1.3819(3)
$\sigma^0_{\rm RS}$ (fb)	24.504(2)	20.825(2)	17.951(2)	13.444(1)	11.965(1)	10.740(1)
$\sigma_{\rm RS}$ (fb)	20.18(3)	19.11(3)	18.09(2)	16.16(2)	15.15(2)	14.24(2)

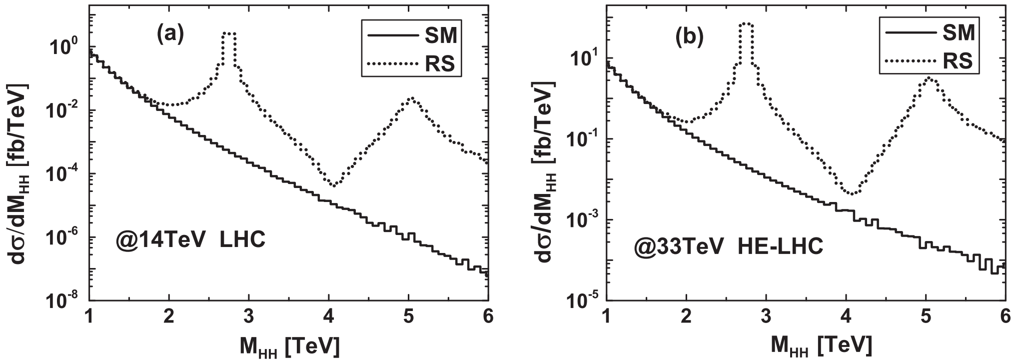

FIG. 5. The Higgs pair invariant mass distributions for the $pp \to HH + X$ process in the SM and RS model at (a) 14 TeV LHC and (b) 33 TeV HE-LHC.

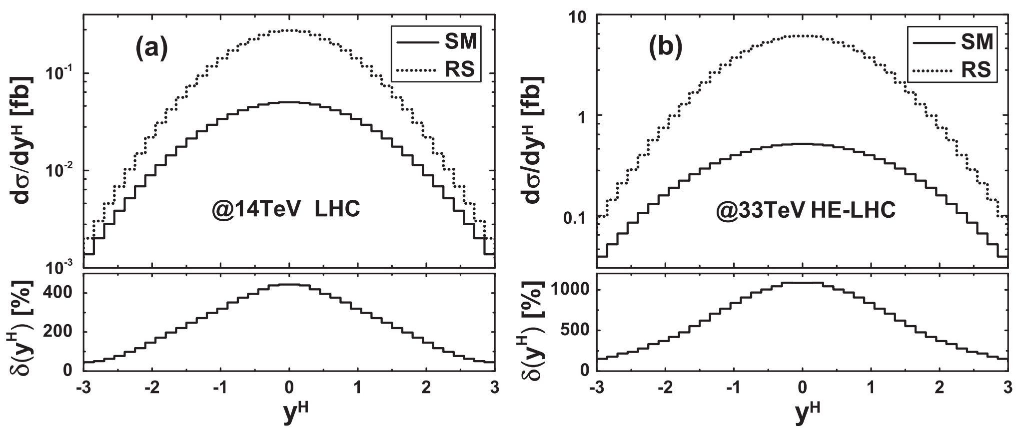

FIG. 6. The final Higgs boson rapidity distributions for the $pp \to HH + X$ process in the SM and RS model at (a) 14 TeV LHC and (b) 33 TeV HE-LHC.

respectively. It shows that the integrated cross sections in both the SM and RS model are sensitive to the factorization/renormalization scale. However, it is more appropriate to take the dynamic factorization/renormalization scale $\mu = \mu_1$ in the calculation of the $pp \to HH + X$ process in the RS model, because the contribution to the double Higgs production at a high energy hadron collider is mainly from the KK graviton resonance when $\sqrt{\hat{s}}$ is larger than KK graviton mass. In the following calculation we take $\mu = \mu_1$.

C. Kinematic distributions

Now we turn to the RS effect on the kinematic distributions of final products. In Figs. 5(a)–5(b) we present the Higgs pair invariant mass distributions for $pp \to HH + X$ in the SM and RS model at the 14 TeV LHC and 33 TeV HE-LHC, respectively. As shown in the figures the SM-like contribution to the M_{HH} distribution is dominant in the low invariant mass region, i.e., $1000\ \mathrm{GeV} < M_{HH} < 1500\ \mathrm{GeV}$. With the increment of M_{HH}, the SM-like contribution decreases significantly and the sensitivity to KK graviton resonance becomes more obvious. This behavior is also shown in Table II. From the two figures we can see that there are two peaks around the masses of the first two KK gravitons, i.e., $M_{HH} \sim M_1 = 2.75$ TeV and $M_{HH} \sim M_2 = 5.04$ TeV, for the M_{HH} distribution in the RS model. It indicates that the resonances of the lightest two KK gravitons contribute to the double Higgs boson production significantly. Therefore, it is possible to apply a mass window cut on the Higgs pair invariant mass to enhance the RS effect.

In Figs. 6(a)–6(b) we depict the rapidity distributions of final Higgs bosons for $pp \to HH + X$ in both the SM and RS model at the 14 TeV LHC and 33 TeV HE-LHC, separately. Since there are two identical Higgs bosons in the final state, we take the rapidities of both final Higgs bosons as entries in the histograms.[2] We define the relative RS effect on the rapidity distribution of final Higgs bosons as $\delta(y^H) = (\frac{d\sigma_{\rm RS}}{dy^H} - \frac{d\sigma_{\rm SM}}{dy^H}) / \frac{d\sigma_{\rm SM}}{dy^H}$. From the figures we see clearly that the Higgs rapidity distributions in both the SM and RS model and the relative RS effect concentrate in the central

[2]The histograms for rapidity as well as transverse momentum distributions of final Higgs bosons (Figs. 6–7) should be divided by 2 for normalization to the total cross section.

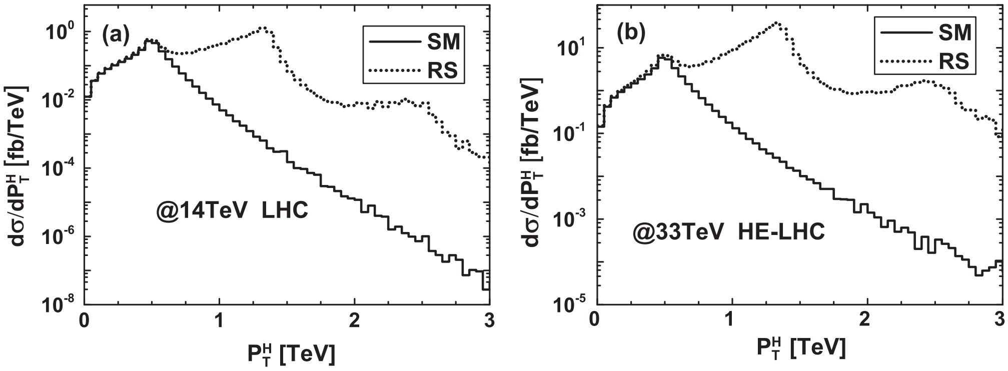

FIG. 7. The final Higgs boson transverse momentum distributions for the $pp \to HH + X$ process in the SM and RS model at (a) 14 TeV LHC and (b) 33 TeV HE-LHC.

rapidity region, and reach their maxima at $y^H = 0$. We can read out from the figures that $\delta(y^H = 0) \sim 443\%$ and 1083% at the 14 TeV LHC and 33 TeV HE-LHC, respectively.

We also present the transverse momentum distributions of final Higgs bosons for $pp \to HH + X$ at the 14 TeV LHC and 33 TeV HE-LHC in Figs. 7(a)–7(b), separately. Similar to the data taking method in Figs. 6(a)–6(b), we pick the transverse momenta of both final Higgs bosons and fill them in the histograms in Figs. 7(a)–7(b). We can see from Figs. 7(a)–7(b) that there are two peaks on each curve for $d\sigma_{\rm RS}/dp_T^H$; one is located at $p_T^H \sim \frac{1}{2} M_1 = 1.375$ TeV and the other, which actually looks like a bulge, is implicitly in the vicinity of $p_T^H \sim \frac{1}{2} M_2 = 2.52$ TeV. As the increment of the pp colliding energy from 14 to 33 TeV, the second bulge stands out and the RS effect is enhanced in the high p_T^H region. From all the distributions in Figs. 5(a)–5(b), Figs. 6(a)–6(b), and Figs. 7(a)–7(b), we can see clearly that the RS effect is significant in some kinematic regions, such as $M_{HH} \sim M_{1,2}$, $y^H \sim 0$, and $p_T^H \sim \frac{1}{2} M_{1,2}$.

D. RS model parameter dependence

We investigate the dependence of the integrated cross section for $pp \to HH + X$ on the RS model parameters M_1 and c_0. In our discussion we take $c_0 = 0.03, 0.05, 0.07, 0.1$, and vary M_1 in the range of [1.5,3.0] TeV. The integrated cross sections at the 14 TeV LHC and 33 TeV HE-LHC are depicted in Figs. 8(a)–8(b), respectively. The horizontal full lines correspond to the cross sections in the SM. From the figures we see that the integrated cross section in the RS model decreases with the increment of the first KK graviton mass M_1. For instance, we can read out from the curves for $c_0 = 0.03$ that the integrated cross sections in the RS model can reach 2.02 and 27.44 fb at $M_1 = 1.5$ TeV, and decrease to 0.160 and 2.46 fb at $M_1 = 3.0$ TeV, which are almost the same as the corresponding SM predictions, at the 14 TeV LHC and 33 TeV HE-LHC, respectively. We also see that the integrated cross section in the RS model is reduced obviously with the decrement of the effective coupling c_0. When $M_1 = 2.75$ TeV, $c_0 = 0.03, 0.05, 0.07$, and 0.1, the relative RS effects for the $pp \to HH + X$ process at the 14 TeV LHC (33 TeV HE-LHC) are 30.5% (72.0%), 84.8% (199%), 166% (391%), and 336% (791%), correspondingly.

E. Double Higgs boson production with semileptonic decay

We consider the Higgs pair production with subsequent Higgs boson decays by employing the narrow width

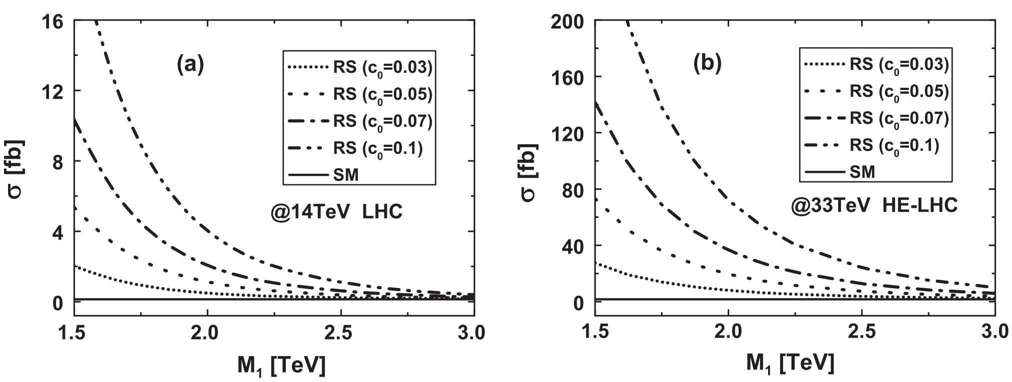

FIG. 8. The integrated cross sections for the $pp \to HH + X$ process as functions of the first KK graviton mass M_1 with $c_0 = 0.03$, 0.05, 0.07, and 0.1 at (a) 14 TeV LHC and (b) 33 TeV HE-LHC.

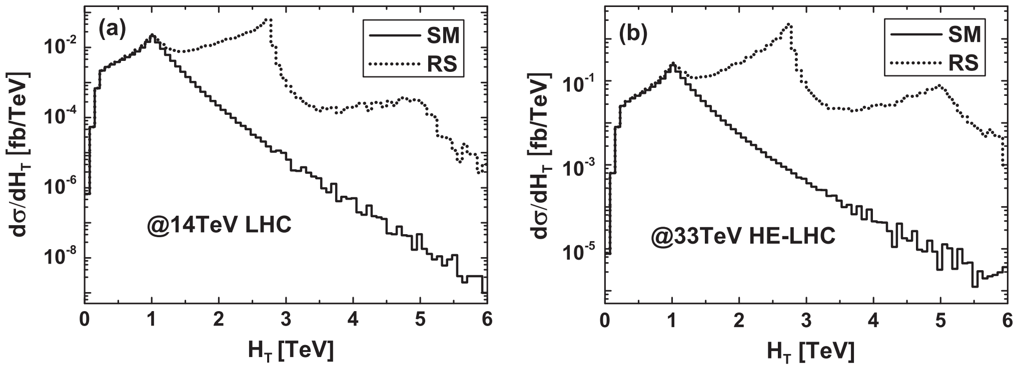

FIG. 9. The H_T distributions for the $pp \to HH \to b\bar{b}\tau^+\tau^- + X$ process in the SM and RS model at (a) 14 TeV LHC and (b) 33 TeV HE-LHC.

approximation. The Higgs decay channels are chosen as one Higgs boson decay to $b\bar{b}$ and the other to $\tau^+\tau^-$. The branching ratios are obtained as $Br(H \to b\bar{b}) = 59.29\%$ and $Br(H \to \tau^+\tau^-) = 5.782\%$ by using the HDECAY program. In Figs. 9(a)–9(b), we demonstrate the H_T distributions for the signal process $pp \to HH \to b\bar{b}\tau^+\tau^- + X$ in the SM and RS model at the 14 TeV LHC and 33 TeV HE-LHC, respectively, where $H_T = \sum_i |\vec{p}_T(i)|$ is the scalar sum of the transverse momenta of final quarks and leptons, i.e., b, $\bar{b}$, τ^+, and τ^-. From the two figures we find that the H_T distribution in the RS model has two peaks at $H_T \sim M_1$ and $H_T \sim M_2$, and behaves similarly to the M_{HH} distribution in the RS model. We also see that the H_T distribution in the SM declines seriously with the increment of H_T in the region of $H_T > 1000$ GeV.

The separation between τ^+ and τ^- on the rapidity-azimuthal-angle plane is defined as $\Delta R_{\tau^+\tau^-} = \sqrt{\Delta y^2 + \Delta\phi^2}$, where Δy and $\Delta\phi$ are the differences of rapidity and azimuthal angle between τ^+ and τ^-. We depict the $\Delta R_{\tau^+\tau^-}$ distributions for $pp \to HH \to b\bar{b}\tau^+\tau^- + X$ in the SM and RS model at the 14 TeV LHC and 33 TeV HE-LHC in Figs. 10(a)–10(b), separately. From the figures we see that the RS effect is quite significant in the region of $\Delta R_{\tau^+\tau^-} < 0.4$ and reaches its maximum at $\Delta R_{\tau^+\tau^-} \sim 0.2$, but is rather small and can be neglected when $\Delta R_{\tau^+\tau^-} > 0.9$. This characteristic is due to the fact that the RS effect mainly comes from the resonant KK graviton production, in which the final Higgs bosons are energetic and therefore the separation between the sequentially produced τ^+ and τ^- is small. It is foreseeable that the distribution of the separation between b and $\bar{b}$ is almost the analogue to the distribution between τ^+ and τ^-, and therefore is not given in this paper.

We also plot the transverse momentum distributions of final τ^+ for $pp \to HH \to b\bar{b}\tau^+\tau^- + X$ in the SM and RS model at the 14 TeV LHC and 33 TeV HE-LHC in Figs. 11(a)–11(b), separately. Unlike the p_T^H distribution where the RS effect is obvious in high p_T^H region, the RS effect on the $p_T^{\tau^+}$ distribution is significant in the whole plotted $p_T^{\tau^+}$ region, and becomes larger and larger with the increment of $p_T^{\tau^+}$ in the region of $p_T^{\tau^+} < 1350$ GeV. The SM-like contribution is negligible when $p_T^{\tau^+} > 750$ GeV.

In detecting the RS effect on the $pp \to HH \to b\bar{b}\tau^+\tau^- + X$ process at the LHC or HE-LHC, we should suppress the accompanied SM backgrounds. The main backgrounds to the RS effect on Higgs pair production are the $pp \to ZZ \to b\bar{b}\tau^+\tau^- + X$, $pp \to ZH \to b\bar{b}\tau^+\tau^- + X$, $pp \to t\bar{t} \to b\bar{b}\tau^+\tau^-\nu_\tau\bar{\nu}_\tau + X$ processes, as well as the SM

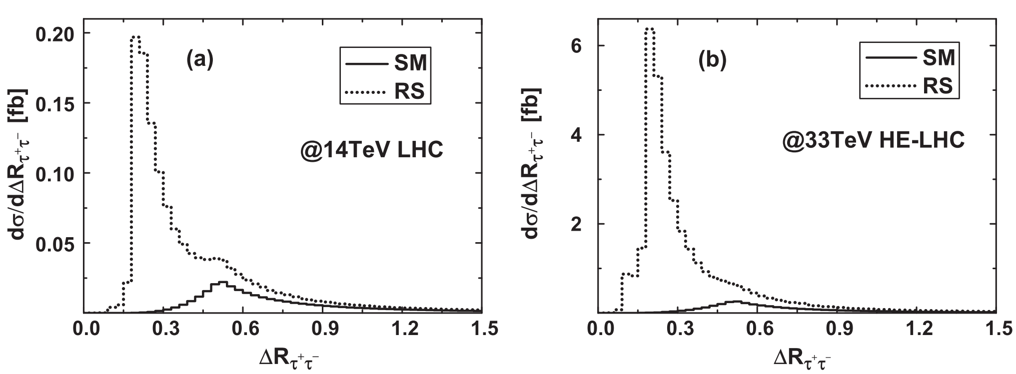

FIG. 10. The $\Delta R_{\tau^+\tau^-}$ distributions for the $pp \to HH \to b\bar{b}\tau^+\tau^- + X$ process in the SM and RS model at (a) 14 TeV LHC and (b) 33 TeV HE-LHC.

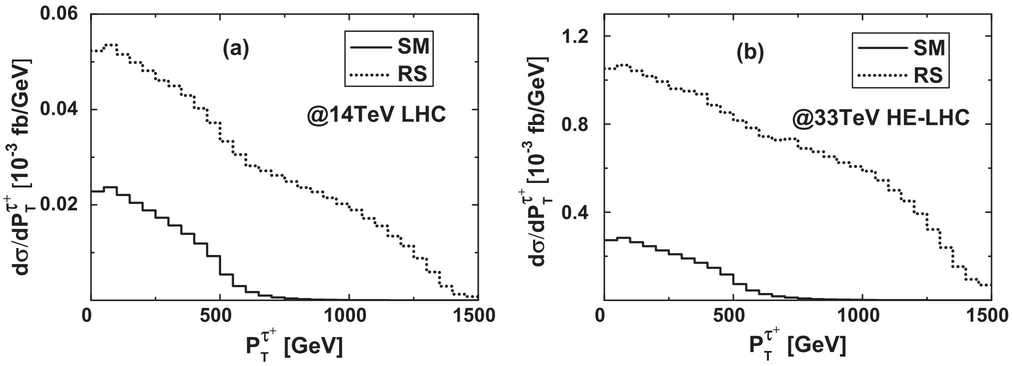

FIG. 11. The transverse momentum distributions of τ^+ for the $pp \to HH \to b\bar{b}\tau^+\tau^- + X$ process in the SM and RS model at (a) 14 TeV LHC and (b) 33 TeV HE-LHC.

contribution to the $pp \to HH \to b\bar{b}\tau^+\tau^- + X$ process. The mass difference between the Z boson and Higgs boson is about 35 GeV; therefore, almost all the $b\bar{b}\tau^+\tau^-$ events from ZZ and ZH productions can be excluded by applying the invariant mass cuts of $|M_{b\bar{b}} - M_H| \leq 20$ GeV and $|M_{\tau^+\tau^-} - M_H| \leq 20$ GeV simultaneously. For $t\bar{t}$ production with subsequent decays $t \to W^+b \to \tau^+\nu_\tau b$ and $\bar{t} \to W^-\bar{b} \to \tau^-\bar{\nu}_\tau\bar{b}$, we apply $p_T^{\rm miss} < 50$ GeV on the missing transverse momentum in the final state to suppress this background. In Table IV we list the signal event numbers (S), significances ($\frac{S}{\sqrt{S+B}}$), and relative RS effects for $pp \to HH \to b\bar{b}\tau^+\tau^- + X$ at the 14 TeV LHC and 33 TeV HE-LHC with integrated luminosities of $\mathcal{L} = 600$ and 1500 fb^{-1}. For $M^{\rm cut}_{b\bar{b}\tau^+\tau^-} = 0$, the relative RS effects are 3.15% and 14.75% and the signal significances are about 4.7(7.4) and 13.1(20.8) for $\mathcal{L} = 600$ fb^{-1} (1500 fb^{-1}) at the 14 TeV LHC and 33 TeV HE-LHC, respectively. With the increment of $M^{\rm cut}_{b\bar{b}\tau^+\tau^-}$, the signal event number declines seriously while the significance raises at first and then declines. However, the relative RS effect increases with the increment of

TABLE IV. The signal event numbers, significances and relative RS effects for $pp \to HH \to b\bar{b}\tau^+\tau^- + X$ at the 14 TeV LHC and 33 TeV HE-LHC with $\mathcal{L} = 600$ and 1500 fb^{-1}.

$\sqrt{S} = 14$ TeV					
$M^{\rm cut}_{b\bar{b}\tau^+\tau^-}$ (GeV)	S		$\frac{S}{\sqrt{S+B}}$		$\delta(\%)$
	$\mathcal{L} = 600$ fb^{-1}	$\mathcal{L} = 1500$ fb^{-1}	$\mathcal{L} = 600$ fb^{-1}	$\mathcal{L} = 1500$ fb^{-1}	
0	631	1577	4.7	7.4	3.15
300	621	1552	6.4	10.0	3.21
400	436	1090	13.6	21.5	4.62
500	**207**	**518**	**12.9**	**20.3**	**10.22**
600	102	255	9.7	15.4	23.09
700	58	144	7.5	11.9	49.6
800	38	96	6.2	9.7	99.4
900	29	73	5.4	8.5	188
1000	**25**	**62**	**5.0**	**7.9**	**336**

$\sqrt{S} = 33$ TeV					
$M^{\rm cut}_{b\bar{b}\tau^+\tau^-}$ (GeV)	S		$\frac{S}{\sqrt{S+B}}$		$\delta(\%)$
	$\mathcal{L} = 600$ fb^{-1}	$\mathcal{L} = 1500$ fb^{-1}	$\mathcal{L} = 600$ fb^{-1}	$\mathcal{L} = 1500$ fb^{-1}	
0	4319	10797	13.1	20.8	14.75
300	4269	10672	17.4	27.5	14.92
400	3279	8198	37.8	59.8	20.33
500	**1926**	**4814**	**39.9**	**63.0**	**40.36**
600	1230	3074	34.4	54.4	81.81
700	905	2262	30.0	47.4	157
800	747	1869	27.3	43.2	285
900	667	1667	25.8	40.8	485
1000	**623**	**1557**	**25.0**	**39.5**	**791**

$M^{\rm cut}_{b\bar{b}\tau^+\tau^-}$. As the increment of $M^{\rm cut}_{b\bar{b}\tau^+\tau^-}$ to 500 GeV, the signal event number drops to 207(518) and 1926(4814) for $\mathcal{L} = 600$ fb^{-1} (1500 fb^{-1}) at the 14 TeV LHC and 33 TeV HE-LHC, separately, but the RS effect could remain at a visible level and the signal significance is also prominent. If we take a more stringent constraint of $M_{b\bar{b}\tau^+\tau^-} > 1000$ GeV, which is not the optimum invariant mass cut for signal significance, the relative RS effects can reach about 336% and 791% at the 14 TeV LHC and 33 TeV HE-LHC, respectively. Therefore, we conclude that the double Higgs production is a promising process to explore the RS effect at the LHC and HE-LHC.

V. SUMMARY

In this work we study the possible Randall-Sundrum effect on the double Higgs boson production at the 14 TeV LHC and 33 TeV HE-LHC. We consider only the lightest two KK gravitons that provide the dominant contribution to the RS effect. We present the integrated cross sections and some kinematic distributions of final products in both the SM and RS model. The results show that the relative RS effect in the vicinities of $M_{HH} \sim M_1$, M_2 or in the central Higgs rapidity region is quite significant. We find that with the increment of $M^{\rm cut}_{HH}$, the integrated cross section in the SM declines more quickly than that in the RS model and then the relative RS effect becomes significant. We conclude that with proper kinematic cuts the double Higgs boson production process is promising in detecting the RS effect. We also investigate the dependence of the integrated cross section on the RS model parameters M_1 and c_0, and find that the integrated cross section is reduced obviously with the increment of the first KK graviton mass M_1 or the decrement of the effective coupling c_0. We find that if we take $pp \to HH \to b\bar{b}\tau^+\tau^- + X$ as the signal process to probe the RS effect, it is possible to extract the RS effect on the signal events from the heavy SM background by choosing proper kinematic cuts on final particles.

ACKNOWLEDGMENTS

This work was supported in part by the National Natural Science Foundation of China (Grants No. 11275190, No. 11375008, No. 11375171, and No. 11405173) and the Fundamental Research Funds for the Central Universities (Grant No. WK2030040044).

APPENDIX: THE RELEVANT FEYNMAN RULES

The relevant RS couplings [14] used in our calculation are listed below:

(i) $G^{\mu\nu}_{KK}(k_3) - H(k_1) - H(k_2)$ vertex:

$$-i\frac{1}{\Lambda_\pi}[\eta^{\mu\nu}(m_H^2 + k_1\cdot k_2) - k_1^\mu k_2^\nu - k_1^\nu k_2^\mu]; \quad \text{(A1)}$$

(ii) $G^{\mu\nu}_{KK}(k_3) - \bar{\psi}(k_1) - \psi(k_2)$ vertex:

$$-i\frac{1}{4\Lambda_\pi}[\gamma^\mu(k_1+k_2)^\nu + \gamma^\nu(k_1+k_2)^\mu - 2\eta^{\mu\nu}(\not{k}_1 + \not{k}_2 - 2m_\psi)]; \quad \text{(A2)}$$

(iii) $G^{\mu\nu}_{KK}(k_4) - \bar{\psi}(k_1) - \psi(k_2) - A^{a\rho}(k_3)$ vertex:

$$ig_s\frac{1}{2\Lambda_\pi}[\gamma^\mu\eta^{\nu\rho} + \gamma^\nu\eta^{\mu\rho} - 2\gamma^\rho\eta^{\mu\nu}]T^a; \quad \text{(A3)}$$

(iv) $G^{\mu\nu}_{KK}(k_3) - A^{a\rho}(k_1) - A^{b\sigma}(k_2)$ vertex:

$$i\frac{2}{\Lambda_\pi}\delta^{ab}[(C^{\mu\nu\rho\sigma\tau\beta} - C^{\mu\nu\rho\beta\sigma\tau})k_{1\tau}k_{2\beta} + \frac{1}{\xi}E^{\mu\nu\rho\sigma}(k_1,k_2)]; \quad \text{(A4)}$$

(v) $G^{\mu\nu}_{KK}(k_4) - A^{a\rho}(k_1) - A^{b\sigma}(k_2) - A^{c\lambda}(k_3)$ vertex:

$$\frac{2}{\Lambda_\pi}g_s f^{abc}[(k_1-k_3)_\tau C^{\mu\nu\tau\sigma\rho\lambda} + (k_2-k_1)_\tau C^{\mu\nu\sigma\rho\tau\lambda} + (k_3-k_2)_\tau C^{\mu\nu\lambda\sigma\tau\rho}]; \quad \text{(A5)}$$

(vi) $G^{\mu\nu}_{KK}(k_5) - A^{a\rho}(k_1) - A^{b\sigma}(k_2) - A^{c\lambda}(k_3) - A^{d\delta}(k_4)$ vertex:

$$-i\frac{1}{\Lambda_\pi}g_s^2[f^{eac}f^{ebd}D^{\mu\nu\rho\sigma\lambda\delta} + f^{eab}f^{ecd}D^{\mu\nu\rho\lambda\sigma\delta} + f^{ead}f^{ebc}D^{\mu\nu\rho\sigma\delta\lambda}]; \quad \text{(A6)}$$

(vii) $G^{\mu\nu}_{KK}(k_3) - \bar{\eta}^a(k_1) - \eta^b(k_2)$ vertex:

$$-i\frac{2}{\Lambda_\pi}\delta^{ab}B^{\alpha\beta\mu\nu}k_{1\alpha}k_{2\beta}; \quad \text{(A7)}$$

(viii) $G^{\mu\nu}_{KK}(k_4) - \bar{\eta}^a(k_1) - \eta^b(k_2) - A^{c\rho}(k_3)$ vertex:

$$\frac{2}{\Lambda_\pi}g_s f^{abc}B^{\alpha\rho\mu\nu}k_{1\alpha}, \quad \text{(A8)}$$

where $G^{\mu\nu}_{KK}$, H, ψ, $A^{a\rho}$, and η^a represent the fields of the RS KK graviton, Higgs boson, fermion, gluon, and ghost for gluon, respectively. In our calculation we adopt the Feynman gauge, i.e., $\xi = 1$. The tensor coefficients $B^{\mu\nu\alpha\beta}$, $C^{\rho\sigma\mu\nu\alpha\beta}$, $D^{\mu\nu\rho\sigma\lambda\delta}$, and $E^{\mu\nu\rho\sigma}(k_1,k_2)$ are expressed as [24]

$$B^{\mu\nu\alpha\beta} = \frac{1}{2}(\eta^{\mu\nu}\eta^{\alpha\beta} - \eta^{\mu\alpha}\eta^{\nu\beta} - \eta^{\mu\beta}\eta^{\nu\alpha}),$$
$$C^{\rho\sigma\mu\nu\alpha\beta} = \frac{1}{2}[\eta^{\rho\sigma}\eta^{\mu\nu}\eta^{\alpha\beta} - (\eta^{\rho\mu}\eta^{\sigma\nu}\eta^{\alpha\beta} + \eta^{\rho\nu}\eta^{\sigma\mu}\eta^{\alpha\beta} + \eta^{\rho\alpha}\eta^{\sigma\beta}\eta^{\mu\nu} + \eta^{\rho\beta}\eta^{\sigma\alpha}\eta^{\mu\nu})],$$
$$D^{\mu\nu\rho\sigma\lambda\delta} = \eta^{\mu\nu}(\eta^{\rho\sigma}\eta^{\lambda\delta} - \eta^{\rho\delta}\eta^{\lambda\sigma}) + [\eta^{\mu\rho}\eta^{\nu\delta}\eta^{\lambda\sigma} + \eta^{\mu\lambda}\eta^{\nu\sigma}\eta^{\rho\delta} - \eta^{\mu\rho}\eta^{\nu\sigma}\eta^{\lambda\delta} - \eta^{\mu\lambda}\eta^{\nu\delta}\eta^{\rho\sigma} + (\mu \leftrightarrow \nu)],$$
$$E^{\mu\nu\rho\sigma}(k_1, k_2) = \eta^{\mu\nu}(k_1^\rho k_1^\sigma + k_2^\rho k_2^\sigma + k_1^\rho k_2^\sigma) - [\eta^{\nu\sigma}k_1^\mu k_1^\rho + \eta^{\nu\rho}k_2^\mu k_2^\sigma + (\mu \leftrightarrow \nu)]. \tag{A9}$$

[1] N. Arkani-Hamed, S. Dimopoulos, and G. Dvali, Phys. Lett. B **429**, 263 (1998); Phys. Rev. D **59**, 086004 (1999); I. Antoniadis, N. Arkani-Hamed, S. Dimopoulos, and G. Dvali, Phys. Lett. B **436**, 257 (1998).
[2] L. Randall and R. Sundrum, Phys. Rev. Lett. **83**, 3370 (1999).
[3] G. Aad *et al.* (ATLAS Collaboration), Phys. Lett. B **716**, 1 (2012); S. Chatrchyan *et al.* (CMS Collaboration), Phys. Lett. B **716**, 30 (2012).
[4] J. Grigo, J. Hoff, K. Melnikov, and M. Steinhauser, Nucl. Phys. **B875**, 1 (2013).
[5] D. de Florian and J. Mazzitelli, Phys. Rev. Lett. **111**, 201801 (2013).
[6] H. Sun, W.-G. Ma, Y.-J. Zhou, Y.-B. Sun, R.-Y. Zhang, and H.-S. Hou, Commun. Theor. Phys. **41**, 73 (2004).
[7] L. Wang, W. Wang, J.-M. Yang, and H. Zhang, Phys. Rev. D **76**, 017702 (2007).
[8] H. de Sandes and R. Rosenfeld, Phys. Lett. B **659**, 323 (2008).
[9] C. S. Kim, K. Y. Lee, and J. Song, Phys. Rev. D **64**, 015009 (2001).
[10] H. Sun and Y.-J. Zhou, J. High Energy Phys. 11 (2012) 127.
[11] L.-S. Ling, R.-Y. Zhang, W.-G. Ma, L. Guo, W.-H. Li, and X.-Z. Li, Phys. Rev. D **89**, 073001 (2014).
[12] W.-H. Li, R.-Y. Zhang, W.-G. Ma, L. Guo, L.-S. Ling, and X.-Z. Li, Phys. Rev. D **89**, 075011 (2014).
[13] H. Davoudiasl, J. L. Hewett, and T. G. Rizzo, Phys. Rev. Lett. **84**, 2080 (2000); Phys. Rev. D **63**, 075004 (2001).
[14] P. Jain and S. Panda, J. High Energy Phys. 03 (2004) 011; E. Dvergsnes, P. Osland, and N. Ozturk, Phys. Rev. D **67**, 074003 (2003); T. Buanes, E. W. Dvergsnes, and P. Osland, Eur. Phys. J. C **35**, 555 (2004); X.-Z. Li, W.-G. Ma, R.-Y. Zhang, and L. Guo, Phys. Rev. D **87**, 056008 (2013).
[15] E. De Pree and M. Sher, Phys. Rev. D **73**, 095006 (2006); M. Arai, N. Okada, K. Smolek, and V. Simak, Phys. Rev. D **75**, 095008 (2007); J. Gao, C.-S. Li, B.-H. Li, H.-X. Zhu, and C.-P. Yuan, Phys. Rev. D **82**, 014020 (2010).
[16] S. Lola, P. Mathews, S. Raychaudhuri, and K. Sridhar, arXiv:hep-ph/0010010.
[17] G. F. Giudice, R. Rattazzi, and J. D. Wells, Nucl. Phys. **B544**, 3 (1999); T. Han, J. D. Lykken, and R.-J. Zhang, Phys. Rev. D **59**, 105006 (1999).
[18] B. W. Harris and J. F. Owens, Phys. Rev. D **65**, 094032 (2002).
[19] T. Kinoshita, J. Math. Phys. (N.Y.) **3**, 650 (1962); T. D. Lee and M. Nauenberg, Phys. Rev. **133**, B1549 (1964).
[20] K. A. Olive *et al.* (Particle Data Group), Chin. Phys. C **38**, 090001 (2014).
[21] CMS Collaboration, Report No. CMS-PAS-HIG-13-005.
[22] A. Martin, W. Stirling, R. Thorne, and G. Watt, Eur. Phys. J. C **63**, 189 (2009).
[23] G. Aad *et al.* (ATLAS Collaboration), Phys. Rev. D **90**, 052005 (2014).
[24] X.-Z. Li, P.-F. Duan, W.-G. Ma, R.-Y. Zhang, and L. Guo, Phys. Rev. D **86**, 095008 (2012); Y.-M. Bai, L. Guo, X.-Z. Li, W.-G. Ma, and R.-Y. Zhang, Phys. Rev. D **85**, 016008 (2012).